Atmospheric Boundary Layer Parameterization

Learning Objectives

Following this lecture, students will be able to:

- Describe the physical mechanisms that result in turbulence in the atmospheric boundary layer and how they vary between unstable (e.g., day) and stable (e.g., night) conditions.
- Define what is meant by turbulence closure and describe the differences between local and non-local closure approaches.
- Describe how eddy-diffusivity, countergradient, and mass-flux approaches parameterize turbulent vertical mixing and the conditions under which each are typically used.
- Recognize how other investigators have designed experiments to test hypotheses relating to how atmospheric boundary layer parameterizations influence a desired forecast element.

Reference Materials

The following lecture material draws extensively from Chapter 5 of *Parameterization Schemes* by David Stensrud, which the course textbook reasonably summarizes. The discussion of eddy-diffusivity mass-flux turbulence parameterizations draws from Siebesma et al. (2007, *J. Atmos. Sci.*), Han et al. (2016, *Wea. Forecasting*), and Han and Bretherton (2019, *Wea. Forecasting*). Finally, *An Introduction to Boundary Layer Meteorology* by Roland Stull is a recommended reference for more details of the physics and dynamics of boundary-layer processes and is often cited by the Stensrud text.

Overview of the Atmospheric Boundary Layer

The *atmospheric boundary layer*, or ABL, is the layer over which the influence of the Earth's surface is directly transmitted to the free atmosphere. The ABL is referred to as the planetary boundary layer over land and the marine or maritime boundary layer over water. The vertical extent of turbulent mixing defines the top of the ABL; it can extend upward of several kilometers above the surface during the local daytime hours but be confined to within 100 m or less of the surface at night. An *inversion* often separates the ABL from the free atmosphere.

The ABL is a turbulent, mixed layer characterized by sub-grid-scale turbulent eddies that transport heat, moisture, and momentum vertically. Turbulent eddies may result from either *buoyancy* or *vertical wind shear*.

Buoyancy refers to the local instability generated by sensible and latent heat fluxes directed from the underlying surface to the atmosphere. The magnitude of these heat fluxes is strongly dependent upon underlying surface characteristics. The release of the local instability results in the generation of *thermals*, or vertical plumes of buoyant air, extending over the depth of the ABL. The upward momentum possessed by thermals enables them to overshoot their level of neutral buoyancy, which is typically found at the top of the ABL where potential temperature rapidly increases with height. The ABL entrains environmental air from the free atmosphere across this inversion as thermals sink back into the ABL. Turbulence in the ABL itself ensures that air from the free atmosphere is quickly mixed with the air that comprises the ABL.

Buoyancy is the primary contributor to ABL turbulence during the local daytime hours. At night, however, vertical wind shear is the primary contributor to ABL turbulence, which is known as *mechanical* turbulence. Although vertical wind shear may contribute to turbulence during the local daytime, buoyancy does not contribute to ABL turbulence during the local nighttime when radiative cooling dominates the surface radiation budget. Mechanical turbulence is intermittent relative to the more continuous turbulence in the buoyancy-driven daytime ABL.

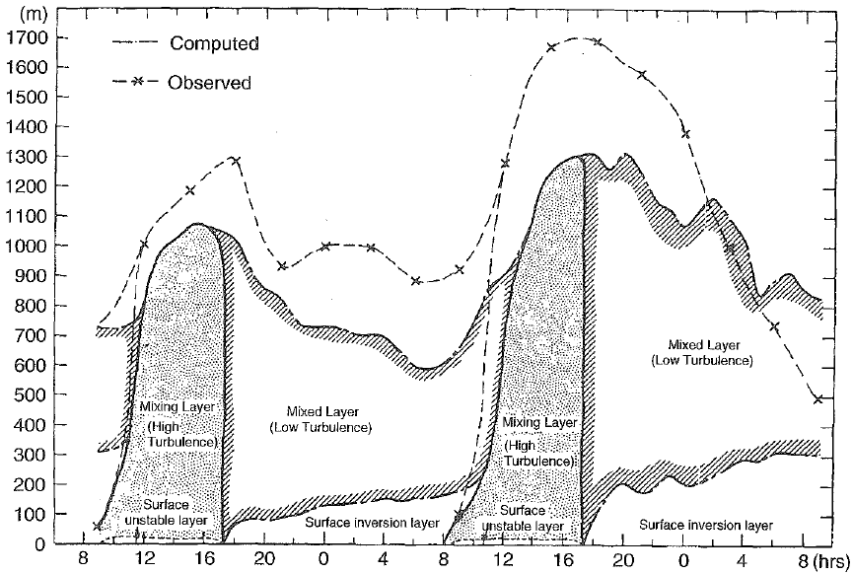

Figure 1. Schematic of ABL evolution over the course of two full diurnal cycles. During the local daytime, the turbulent mixed layer grows to over 1 km in depth. ABL turbulence weakens as day turns to night, leaving behind a residual mixed layer atop a near-surface inversion layer that forms in response to radiative cooling. The near-surface inversion layer deepens slowly at night as the effects of radiative cooling are episodically interrupted by mechanical turbulence. At the same time, the residual mixed layer shrinks in vertical extent due to internal friction as the evening progresses. Figure reproduced from Stensrud (2007), their Fig. 5.1.

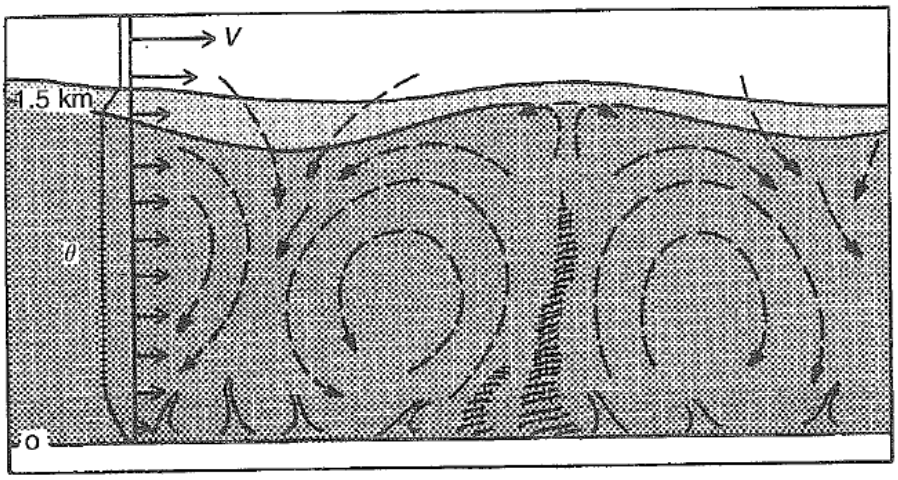

Figure 2. Artistic rendering of an idealized daytime ABL. Here, organized thermals act in concert with turbulent eddies to homogenize potential temperature, momentum, and moisture within the ABL. Entrainment occurs at the top of the ABL as thermals overshoot their level of neutral buoyancy and subsequently sink back into the ABL. Subtle horizontal variations in ABL height are also depicted. Figure reproduced from Stensrud (2007), their Fig. 5.5.

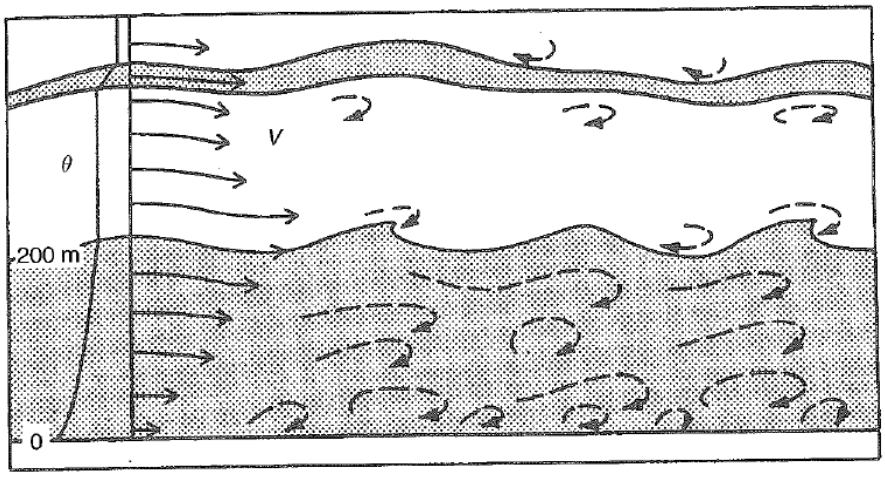

Figure 3. Artistic rendering of an idealized nocturnal ABL. Note its reduced depth (~200 m) relative to the daytime ABL in Fig. 2 (~1500 m). In the nocturnal ABL, turbulence results exclusively from vertical wind shear. A pronounced low-level jet exists atop the nocturnal ABL and is theorized to result from inertial oscillations induced by an imbalance between the Coriolis and horizontal pressure gradient forces that develops as radiative cooling acts to decouple the surface layer from the atmosphere above. Gravity waves trapped beneath the near-surface inversion are superimposed upon the mean flow, and the weakly turbulent residual mixed layer is found above this inversion. Figure reproduced from Stensrud (2007), their Fig. 5.7.

The evolution of the ABL over a series of several diurnal cycles is illustrated in Fig. 1. Idealized schematics of the daytime and nocturnal ABLs are provided in Figs. 2 and 3, respectively. A boundary-layer parameterization must be able to accurately reproduce both daytime and nocturnal ABLs under a wide range of atmospheric conditions.

Why do we care about the ABL? Vertical mixing in the ABL influences surface temperature and moisture. Indeed, a common rule of thumb for forecasting high temperatures during sunny days in the warm season is to follow a dry adiabat from the midday forecast 850 hPa temperature down to the surface. Since a dry adiabat is a line of constant potential temperature, this rule follows from the principle that vertical mixing acts to homogenize potential temperature in the ABL (as noted in the Fig. 2 caption). If a superadiabatic lapse rate immediately above the surface is anticipated, such as if the underlying soils are dry, then adding 1-2°C to the temperature obtained from this rule often leads to improved results. Vertical mixing also influences lifting and stability parameters such as the lifting condensation level, level of free convection, and CAPE and CIN, in turn influencing diurnal cumulus development and thunderstorm formation. Finally, vertical mixing also influences surface winds, most notably when strong winds are found atop the ABL and strong surface sensible heating occurs.

ABL Structure

The temporal evolution of the daytime ABL is depicted in Fig. 4. Conceptual vertical profiles of potential temperature, momentum, and moisture within the daytime ABL are presented in Fig. 5, while their nighttime ABL counterparts are depicted in Fig. 6.

Vertical mixing in the ABL *homogenizes* potential temperature, mixing ratio, and momentum. For potential temperature, vertical mixing makes its profile uniform by mixing higher potential-temperature air from both the surface (where it is increased during the local daytime by surface sensible heat fluxes) and top of the ABL (where it is increased by entrainment from above the ABL) over the ABL's depth. For mixing ratio, this homogeneity is often slightly offset by the entrainment of drier air at the top of the ABL and increased mixing ratio through surface latent heat fluxes near the surface; thus, mixing ratio typically decreases slightly with increasing altitude in the ABL. For momentum, this homogeneity is often slightly offset by the entrainment of higher momentum air at the top of the ABL and frictional dissipation near the surface. Thus, momentum typically increases slightly with increasing altitude in the ABL.

At night, radiative cooling results in the surface layer decoupling from the mixed layer above. In the resulting stable layer, potential temperature, mixing ratio, and wind speed all typically increase with height. Atop this stable layer is the residual mixed layer, where potential temperature, mixing ratio, and wind speed are approximate constant with height, as in the daytime ABL. As noted in the Fig. 2 caption, the residual layer slowly and episodically shrinks

in depth through the night as the near-surface stable layer deepens (due to continued radiative cooling) and internal friction erodes it from the top-down. Profiles of potential temperature, mixing ratio, and wind speed above the nocturnal ABL, in the free atmosphere, closely resemble their daytime counterparts.

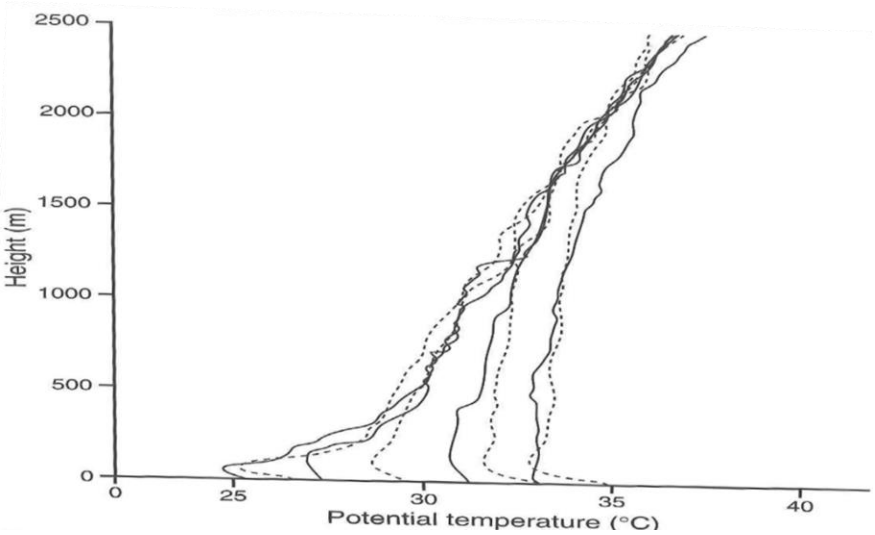

Figure 4. Vertical profiles of potential temperature (°C). Solid lines depict profiles obtained over a salt flat, while dashed lines depict profiles obtained over a vegetated yet sandy location. Profiles taken early (late) on this day are located further to the left (right) on the diagram. Figure reproduced from Warner (2011), their Fig. 4.10.

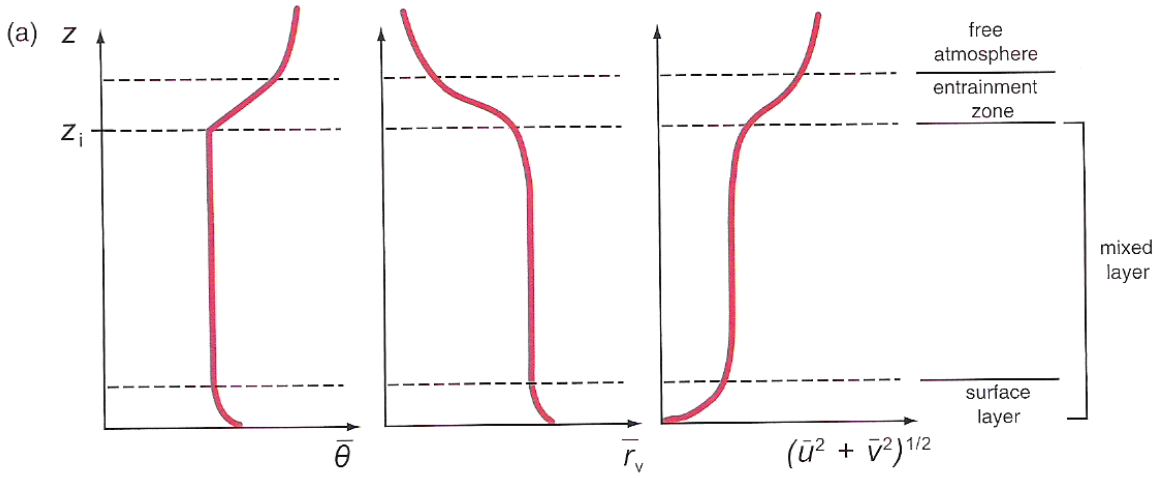

Figure 5. Conceptualized vertical profiles of potential temperature, water vapor mixing ratio, and horizontal wind speed over the depth of the daytime ABL. Figure reproduced from Markowski and Richardson (2010), their Fig. 4.11a.

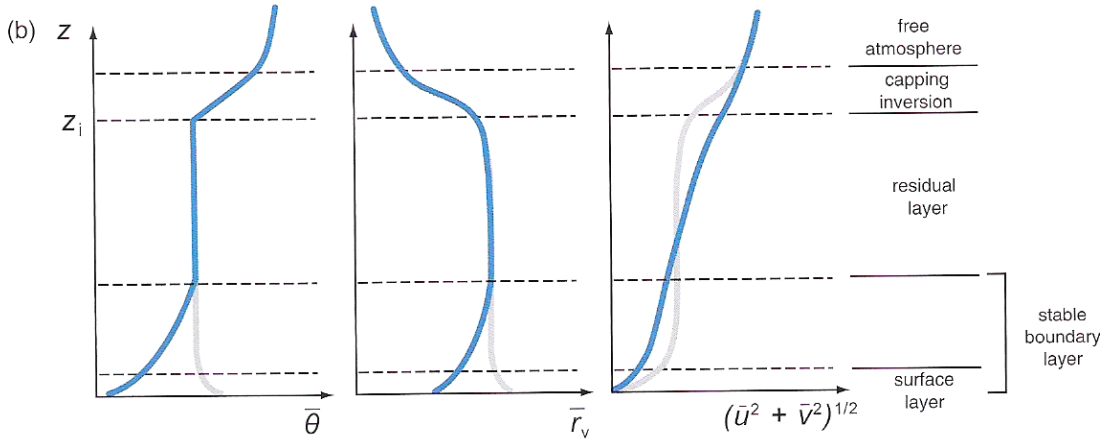

Figure 6. As in Fig. 5, except for the nighttime ABL. Thin grey lines in each panel depict their daytime ABL counterparts for comparison. Figure reproduced from Markowski and Richardson (2010), their Fig. 4.11b.

Three distinct layers exist in the ABL. The discussion to this point has focused on the *mixed layer*, which is the deepest of the three layers in the ABL and that which lies closes to the free atmosphere. Below the mixed layer is the *surface layer*. The surface layer, with a thickness of ~100 m or less, is a layer over which turbulent transports vary little in magnitude with height relative to their variability in the mixed layer. In this layer, potential temperature decreases with height from its relative maximum at the surface (which results from strong sensible heating) and is thus characterized by a superadiabatic lapse rate. Mixing ratio also decreases with height from its relative maximum at the surface (which results from surface latent heat fluxes). Momentum, however, increases with height from its relative minimum at the surface (which results from friction). Surface layer processes are typically parameterized by a surface layer parameterization, which is often developed and tuned to work with a particular ABL parameterization.

Below the surface layer, and thus nearest the surface, is the *laminar sublayer*. Because the wind speed perpendicular to any rigid surface such as the ground must be zero, turbulence cannot exist right at the ground. In the absence of turbulence, some other means of transporting sensible and latent heat fluxes from the underlying surface to the boundary layer must exist. This occurs via molecular mixing in the ~1-mm–thick laminar sublayer. Transport via molecular mixing is downgradient, from high to low values, and thus reduces the vertical gradients in potential temperature and mixing ratio that exist between the surface and the air just above. Physical processes occurring in the laminar sublayer are typically parameterized in one or both of surface layer and land-surface parameterizations.

As stated above, ABL structure is strongly impacted by the characteristics of the underlying surface. This is particularly manifest via the roughness of that surface, given by the *roughness length* (or z_0). The roughness length defines the height above the ground at which the mean wind

speed goes to zero under neutrally stable conditions. Roughness length is relatively small (on the order of mm) over relatively smooth surfaces and is relatively large (on the order of cm or larger) over relatively rough surfaces. The roughness length influences the vertical momentum profile in the surface layer, which in turn influences near-surface turbulent fluxes of heat, moisture, and momentum.

For a well-mixed ABL, the vertical profile of momentum in the surface layer is a log-wind profile, as given by:

$$u(z) = \frac{u*}{k} \ln\left(\frac{z}{z_0}\right)$$

Here, $u*$ is the friction velocity, reflecting the drag (or frictional stress) of the surface against the atmosphere. Both $u*$ and k, the von Karman constant (typically 0.35-0.4), are independent of height. As a result, the horizontal wind speed – and thus momentum – increases logarithmically with increasing height above the ground in the surface layer. Though the log-wind profile explicitly holds only under neutrally stable conditions, similar profiles result from stable and unstable conditions.

Other ABL-Related Concepts

When we think of the ABL, we typically think of the local ABL, that which is in direct engagement with the surface. However, vertical profiles of potential temperature, mixing ratio, and momentum in the local free atmosphere may reflect properties of upstream ABLs that have been advected atop the local ABL by the synoptic-scale flow. These *elevated mixed layers* are most common downwind of large mountain ranges and, to lesser extent, over the tropical North Atlantic Ocean downwind of the Sahara Desert. Boundaries between the local ABL and an elevated mixed layer are known as *internal boundaries*. An ABL parameterization must be able to accurately represent the formation of both the local ABL and the elevated mixed layer, while the numerical model as a whole must be able to accurately depict the downstream transport and evolution of the elevated mixed layer. An idealized schematic of an elevated mixed layer, such as might occur over the Great Plains downwind of the Rocky Mountains, is depicted in Fig. 7.

Finally, although the ABL is governed by local turbulence, larger-scale phenomena regularly emerge from and interact with the local turbulence. The most commonly observed manifestation of larger-scale ABL variability is that associated with *roll circulations*. Rolls are most commonly observed during the daytime ABL during the warm season, when sensible heating is strong, but can also be observed in the nocturnal ABL as well as the daytime ABL during the cold season. Rolls are typically organized parallel to the mean horizontal wind in the ABL and can be analyzed using visible satellite imagery or Doppler radar.

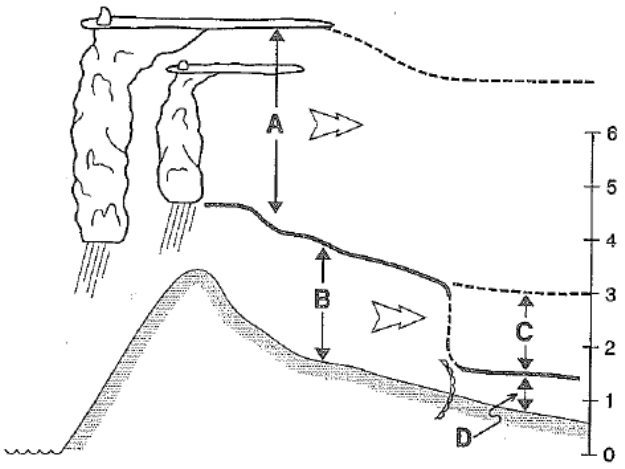

Figure 7. Idealized schematic of some of the complex structures that ABL parameterizations must be able to accurately represent. In this example, a shallow, moist ABL (D) is found ahead of a dryline. Behind the dryline, strong sensible heating results in a deep, well-mixed ABL with low relative humidity (B). The synoptic-scale west-to-east flow advects this layer over that in (D), resulting in the formation of an elevated mixed layer (C). A similar structure results when a mixed layer such as that in (B) is advected over a comparatively cool, moist marine layer. The downstream vertical profile can also be influenced by upstream processes over elevated terrain – here, deep, moist convection and concordant latent heat release (A). Figure reproduced from Stensrud (2007), their Fig. 5.8.

ABL Parameterization: Is It Even Necessary?

Though the above discussion might not indicate this to be the case, the primitive equations are capable of explicitly resolving turbulent motions within the atmosphere if effective radiation and land-surface parameterizations are present within the model (e.g., to represent local buoyancy, surface heat fluxes, and surface drag). However, as turbulent eddies cover a wide range of length scales ranging from tens of meters to a kilometer or more, to do so within a numerical model is computationally expensive. Approaches exist by which an ABL parameterization need not be used, such as large-eddy and direct numerical simulation. The former only explicitly resolves relatively large eddies, whereas the latter explicitly resolves all turbulent flows. Large eddy simulation (LES) has historically been used to guide ABL parameterization development and evaluation (e.g., to aid in determining the functional forms of and coefficients for empirical relationships contained in the overall parameterization). The computational expense of these methods, however, currently limits the extent to which they are used in real-time and most

research-focused simulations. As a result, *an ABL parameterization is needed to represent the resolved-scale impacts of sub-grid-scale turbulence in a numerical simulation*.

An Introduction to ABL Parameterization: Turbulence Closure

Early in the semester, we introduced the concept of *Reynolds' averaging* to rewrite the primitive equations so that they are formally valid only on the scales resolved by the model grid. Recall that a model dependent variable x can be written as the sum of a resolved-scale mean value $\bar{x}$ and a sub-grid-scale perturbation value x'. Substituting this definition into the primitive equations and using Reynolds' postulates to simplify the result allows one to obtain a form of the primitive equations applicable only on the scales resolved by the model grid.

Let us revisit Reynolds' averaging in the context of the v-momentum equation. Neglecting the curvature terms and friction for convenience, the v-momentum equation may be written as:

$$\frac{\partial v}{\partial t} = -u\frac{\partial v}{\partial x} - v\frac{\partial v}{\partial y} - w\frac{\partial v}{\partial z} - \frac{1}{\rho}\frac{\partial p}{\partial y} - 2\Omega u \sin\phi$$

If we rewrite u, v, w, p, and ρ as the sum of their resolved-scale and sub-grid-scale components, noting that $\rho' \approx 0$, then we obtain:

$$\frac{\partial \bar{v}}{\partial t} + \frac{\partial v'}{\partial t} = -\left(\bar{u}+u'\right)\frac{\partial\left(\bar{v}+v'\right)}{\partial x} - \left(\bar{v}+v'\right)\frac{\partial\left(\bar{v}+v'\right)}{\partial y} - \left(\bar{w}+w'\right)\frac{\partial\left(\bar{v}+v'\right)}{\partial z} - \frac{1}{\bar{\rho}}\frac{\partial\left(\bar{p}+p'\right)}{\partial y} - 2\Omega\left(\bar{u}+u'\right)\sin\phi$$

Expanding this equation, we obtain:

$$\frac{\partial \bar{v}}{\partial t} + \frac{\partial v'}{\partial t} = -\bar{u}\frac{\partial \bar{v}}{\partial x} - \bar{u}\frac{\partial v'}{\partial x} - u'\frac{\partial \bar{v}}{\partial x} - u'\frac{\partial v'}{\partial x} - \bar{v}\frac{\partial \bar{v}}{\partial y} - \bar{v}\frac{\partial v'}{\partial y} - v'\frac{\partial \bar{v}}{\partial y} - v'\frac{\partial v'}{\partial y} - \bar{w}\frac{\partial \bar{v}}{\partial z} - \bar{w}\frac{\partial v'}{\partial z} - w'\frac{\partial \bar{v}}{\partial z} - w'\frac{\partial v'}{\partial z}$$
$$- \frac{1}{\bar{\rho}}\frac{\partial \bar{p}}{\partial y} - \frac{1}{\bar{\rho}}\frac{\partial p'}{\partial y} - 2\Omega\bar{u}\sin\phi - 2\Omega u'\sin\phi$$

If we take the Reynolds average of this equation and apply Reynolds' postulates, we obtain:

$$\frac{\partial \bar{v}}{\partial t} = -\bar{u}\frac{\partial \bar{v}}{\partial x} - \bar{v}\frac{\partial \bar{v}}{\partial y} - \bar{w}\frac{\partial \bar{v}}{\partial z} - \overline{u'\frac{\partial v'}{\partial x}} - \overline{v'\frac{\partial v'}{\partial y}} - \overline{w'\frac{\partial v'}{\partial z}} - \frac{1}{\bar{\rho}}\frac{\partial \bar{p}}{\partial y} - 2\Omega\bar{u}\sin\phi$$

The fourth, fifth, and sixth terms on the right-hand side of this equation, which represent the advection of v' by $\mathbf{v}'$ (e.g., advection of turbulent meridional velocity by the turbulent 3-D velocity), may be rewritten using their flux-form definitions:

$$\frac{\partial \overline{u'v'}}{\partial x} = \overline{u'\frac{\partial v'}{\partial x}} + \overline{v'\frac{\partial u'}{\partial x}} \qquad \frac{\partial \overline{v'v'}}{\partial y} = \overline{v'\frac{\partial v'}{\partial y}} + \overline{v'\frac{\partial v'}{\partial y}} \qquad \frac{\partial \overline{w'v'}}{\partial z} = \overline{w'\frac{\partial v'}{\partial z}} + \overline{v'\frac{\partial w'}{\partial z}}$$

But, on turbulent scales of motion, on which the Boussinesq approximation is said to hold, the following continuity equation applies:

$$\frac{\partial u'}{\partial x} + \frac{\partial v'}{\partial y} + \frac{\partial w'}{\partial z} = 0$$

If this equation is multiplied by $-v'$ and Reynolds averaged, we find that three of the six terms in the flux-form expansion above drop out. This allows us to rewrite our *v*-momentum equation:

$$\frac{\partial \bar{v}}{\partial t} = -\bar{u}\frac{\partial \bar{v}}{\partial x} - \bar{v}\frac{\partial \bar{v}}{\partial y} - \bar{w}\frac{\partial \bar{v}}{\partial z} - \frac{\partial \overline{u'v'}}{\partial x} - \frac{\partial \overline{v'v'}}{\partial y} - \frac{\partial \overline{w'v'}}{\partial z} - \frac{1}{\bar{\rho}}\frac{\partial \bar{p}}{\partial y} - 2\Omega\bar{u}\sin\phi$$

Every term in this equation except the fourth, fifth, and sixth terms on the right-hand side is written in terms of only resolved-scale variables. These terms require no parameterization. The remaining terms must be parameterized in some fashion. These terms are often described as *eddy fluxes* (**eddy** = localized, **flux** = transport) and *flux covariances* (the average of the product of the two sub-grid terms provides a measure of how they vary with respect to each other).

In general, ABL parameterizations diagnose all turbulent *vertical* mixing –not just that in the ABL. Turbulent horizontal mixing, such as that which may occur across adjacent grid cells, is typically neglected, such that the $\overline{u'v'}$ and $\overline{v'v'}$ terms above are assumed to be zero.

ABL parameterizations differ in how the vertical mixing term is parameterized. There are two general classes of parameterization approaches:

- Directly parameterize these terms in terms of some empirical relationships between these terms and resolved-scale model variables.
- Develop predictive equations for these terms.

The first of these methods is straightforward to conceptualize, and we will return to it shortly when considering examples of ABL parameterization. In contrast, the second of these methods is not as straightforward to conceptualize. How, exactly, can predictive equations be developed for the covariance terms in the above equation? To do so, we require two forms of the *v*-momentum equation: its final, simplified form and its fully expanded form:

$$\frac{\partial \bar{v}}{\partial t} = -\bar{u}\frac{\partial \bar{v}}{\partial x} - \bar{v}\frac{\partial \bar{v}}{\partial y} - \bar{w}\frac{\partial \bar{v}}{\partial z} - \frac{\partial \overline{u'v'}}{\partial x} - \frac{\partial \overline{v'v'}}{\partial y} - \frac{\partial \overline{w'v'}}{\partial z} - \frac{1}{\bar{\rho}}\frac{\partial \bar{p}}{\partial y} - 2\Omega\bar{u}\sin\phi$$

$$\frac{\partial \bar{v}}{\partial t}+\frac{\partial v'}{\partial t}=-\bar{u}\frac{\partial \bar{v}}{\partial x}-\bar{u}\frac{\partial v'}{\partial x}-u'\frac{\partial \bar{v}}{\partial x}-u'\frac{\partial v'}{\partial x}-\bar{v}\frac{\partial \bar{v}}{\partial y}-\bar{v}\frac{\partial v'}{\partial y}-v'\frac{\partial \bar{v}}{\partial y}-v'\frac{\partial v'}{\partial y}-\bar{w}\frac{\partial \bar{v}}{\partial z}-\bar{w}\frac{\partial v'}{\partial z}-w'\frac{\partial \bar{v}}{\partial z}-w'\frac{\partial v'}{\partial z}$$
$$-\frac{1}{\bar{\rho}}\frac{\partial \bar{p}}{\partial y}-\frac{1}{\bar{\rho}}\frac{\partial p'}{\partial y}-2\Omega\bar{u}\sin\phi-2\Omega u'\sin\phi$$

If we subtract the top equation from the bottom equation, we obtain:

$$\frac{\partial v'}{\partial t}=-\bar{u}\frac{\partial v'}{\partial x}-u'\frac{\partial \bar{v}}{\partial x}-u'\frac{\partial v'}{\partial x}-\bar{v}\frac{\partial v'}{\partial y}-v'\frac{\partial \bar{v}}{\partial y}-v'\frac{\partial v'}{\partial y}-\bar{w}\frac{\partial v'}{\partial z}-w'\frac{\partial \bar{v}}{\partial z}-w'\frac{\partial v'}{\partial z}-\frac{1}{\bar{\rho}}\frac{\partial p'}{\partial y}-2\Omega u'\sin\phi$$
$$+\frac{\partial \overline{u'v'}}{\partial x}+\frac{\partial \overline{v'v'}}{\partial y}+\frac{\partial \overline{w'v'}}{\partial z}$$

This equation can be used in part to obtain equations for the covariance terms. For instance, the general form of a predictive equation for $\overline{u'v'}$ is given by its chain rule expansion:

$$\frac{\partial}{\partial t}\left(\overline{u'v'}\right)=\overline{u'\frac{\partial v'}{\partial t}}+\overline{v'\frac{\partial u'}{\partial t}}$$

The first right-hand side term of this equation can be obtained from the tendency equation for *v'* by multiplying it by *u'*, applying the product rule for partial derivatives, taking a Reynolds average, and simplifying using the continuity equation and Reynolds' postulates. The second right-hand side term can be obtained similarly from the tendency equation for *u'* from an analogous expansion of the *u*-momentum equation.

However, when doing so, triple correlation terms of the form $\overline{u'u'v'}$, $\overline{u'v'v'}$, and $\overline{u'w'v'}$ result. One could follow a similar procedure to obtain predictive equations for the triple correlation terms, but these would contain quadruple correlation terms. Indeed, one can never obtain a predictive equation for a correlation term that does not contain an even higher-order correlation term. At some point, the unknown higher-order correlation terms must be parameterized in terms of the resolved-scale model variables.

The *order* of an ABL parameterization is defined by the lowest order of covariance or correlation terms that are parameterized. A first-order closure means that there exist predictive equations for the resolved-scale model variables while the covariance terms are parameterized. A second-order closure means that there exist predictive equations for the resolved-scale model variables and the covariance terms while the triple correlation terms are parameterized. Higher-order closures follow this same basic pattern. Non-integer closures, wherein a mixture of parameterizations and predictive equations are used to solve for covariance terms, also exist; e.g., a 1.5-order closure will predict some covariance terms and parameterize others. Generally, higher-order closures are thought to be more accurate because they reduce the influence that the parameterized terms have

on the resolved-scale model fields. Higher-order closures also allow for the more accurate specification of the diffusion coefficients for those parameterizations in which vertical mixing is parameterized as being proportional to diffusion coefficients.

Within this hierarchy of ABL parameterization orders is the approach used to parameterize the sub-grid-scale turbulence. Two approaches exist: *local* and *non-local closures*:

- Local closures use only known (resolved) quantities at adjacent vertical grid points to obtain values of unknown quantities.
- Non-local closures use known quantities over the full ABL to obtain values of unknown quantities.

Local closures are formulated under the assumption that turbulent mixing occurs primarily by turbulent eddies of small vertical extent, whereas non-local closures assume that turbulent mixing occurs by eddies of varying vertical extent up to and including the ABL's depth. Two common non-local closures assume (a) turbulent mixing occurs by turbulent eddies of varying depth with roots in the surface layer or (b) turbulent mixing occurs by turbulent eddies of varying depth with roots anywhere within the ABL. Idealized schematics of local and non-local closures are depicted in Fig. 8. The Mellor-Yamada-Janjic and Yonsei University ABL parameterizations are examples of local and non-local closures, respectively. Note that an ABL parameterization need not be exclusively local or non-local; for instance, the ACM2 ABL parameterization is non-local for upward mixing and local for downward mixing.

Further, within the local and non-local closure frameworks, there are three classes of turbulence parameterizations that serve as the basis for the remainder of our background discussion:

- *Eddy-diffusivity*, inherently a local-mixing approach.
- *Eddy-diffusivity countergradient*, where a countergradient approach is used to parameterize non-local transport by large eddies.
- *Eddy-diffusivity mass-flux*, where a mass-flux approach akin to that used by some cumulus parameterizations is used to parameterize non-local transport by surface-based thermals.

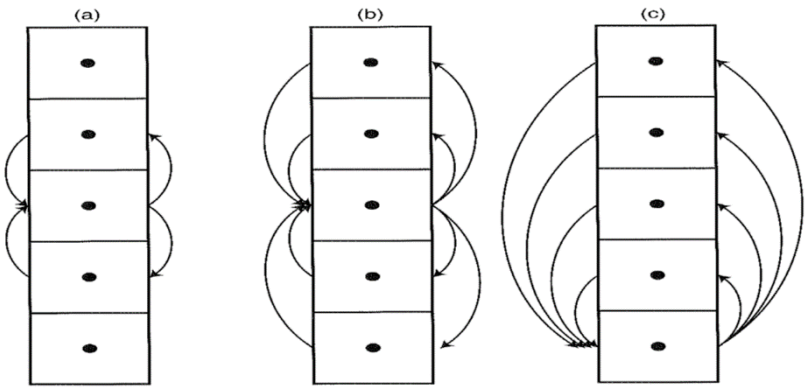

Figure 8. Idealized schematics of vertical mixing associated with (a) local, (b) non-local rooted at any grid cell, and (c) non-local rooted in the surface layer closures. Please see above for more details regarding each closure. Figure reproduced from Warner (2011), their Fig. 4.15.

Eddy-Diffusivity Approaches

As noted above, local turbulence closures use only known quantities at adjacent vertical grid points to obtain values of unknown quantities. They are formulated under the assumption that turbulent mixing occurs primarily by turbulent eddies of small vertical extent.

Recall that turbulent vertical mixing acts to homogenize thermodynamic and kinematic properties. In this sense, it works to reduce the value of local maxima and increase the value of local minima. We introduced explicit diffusion operators earlier this semester using a nearly identical context: to weaken gradients by reducing maxima and increasing minima. This is a convenient framework by which we can understand eddy-diffusivity parameterizations: they mimic turbulent vertical mixing associated with turbulent eddies through explicit diffusion.

To begin, let us assume a first-order local turbulence closure, such that the covariance terms are those that are parameterized, and focus on vertical mixing in the daytime ABL when buoyancy is important. The parameterized covariance term has the form of a zeroth-order diffusion operator:

$$\overline{w'\xi'} = -K\frac{\partial\bar{\xi}}{\partial z}$$

Here, ξ is any model dependent variable (e.g., u, v, θ, q) for which a covariance term exists and K is a diffusion (or mixing) coefficient with units of $m^2\ s^{-1}$. Typically, different values for K are specified for momentum (K_m) and mass (K_h) turbulent mixing.

Local closure parameterizations require some means of specifying the mass (K_h) and momentum (K_m) diffusion coefficients. The precise methods by which these coefficients are specified varies.

For first-order local closures, K_h and K_m are often determined using the so-called *profile* method, wherein they are specified as functions of an empirically determined mixing length scale, vertical wind shear, and stability. For higher-order local closures, the diffusion coefficients are typically also a function of turbulent kinetic energy. Independent of the closure order, LES is typically used to determine the empirical relationships that determine the functions used to specify K_h and K_m, although it is possible to instead use observational datasets to do so.

Similar equations can be obtained for higher-order closure parameterizations; e.g., the left-hand side may be associated with a triple correlation term that is parameterized as a function of the product of a diffusion coefficient with a vertical partial derivative of a resolved double correlation (or covariance) term.

The above equation contains two important insights:

- The covariance term is parameterized as a function of predicted model variables.
- As the partial derivative is defined by the limit as Δz approaches zero (i.e., infinitesimally small Δz), this formulation is inherently local.

To gain insight into this parameterization, let us consider the vertical heat flux, i.e.,

$$\overline{w'\theta'} = -K_h \frac{\partial \bar{\theta}}{\partial z}$$

Let us also consider an idealized vertical profile of $\bar{\theta}$ in the daytime ABL, as in Fig. 5a. In the daytime surface layer, where $\bar{\theta}$ decreases with height due to strong surface sensible heating, the parameterization indicates that $\overline{w'\theta'} > 0$ for $K_h > 0$. This implies a positive correlation between w', representing vertical motions associated with turbulent eddies, and θ'. Turbulence thus acts to move warm air ($\theta' > 0$) upward ($w' > 0$) or cool air downward. This is consistent with what we know about the daytime surface layer: thermals act to transport warmth upward, from relatively high values toward relatively low values.

At the top of the daytime ABL, where there exists an inversion and thus a rapid increase in $\bar{\theta}$ with height, the parameterization indicates that $\overline{w'\theta'} < 0$ for $K_h > 0$. This implies a negative correlation between w' and θ'. Turbulence thus acts to move warm air ($\theta' > 0$) downward ($w' < 0$) or cool air upward. This is consistent with what we know about the daytime mixed layer: turbulent eddies entrain high potential temperature air from above into the boundary layer, again representing transport from relatively high values toward relatively low values.

The above discussion helps to illustrate that, so long as $K > 0$, this parameterized turbulence is associated with *downgradient* transport – i.e., that from high values toward low values. However,

not all turbulent transport within the ABL is downgradient. Consider the case of the late morning ABL, characterized by a residual nocturnal inversion atop a shallow surface superadiabatic layer. In the real atmosphere, warm thermals move heat upward from the surface over the depth of the ABL (e.g., Fig. 2), including through the residual nocturnal inversion. In the context of a local gradient, this can be thought of as *countergradient* transport, or that from low toward high values. However, a first-order local closure instead actually represents this as downgradient downward transport of warm air.

Thus, there is an inconsistency between this parameterization and the underlying physics. This is a problem, as observations of the daytime ABL indicate that most vertical transport of mass and momentum is accomplished by the largest eddies *that are more representative of the properties of the entire ABL rather than of local properties* (i.e., those at adjacent vertical levels). This implicitly indicates that not all vertical transport in the daytime ABL is downgradient. Although higher-order local-closure parameterizations can permit countergradient transport, they cannot permit large eddies and thus are a crude approximation to the underlying physics.

Returning to Fig. 5a, let us consider the daytime mixed layer. Here, where $\bar{\theta}$ is approximately constant with height, the parameterization indicates that $\overline{w'\theta'} \approx 0$ for $K_h > 0$. This implies no vertical heat flux – and thus no turbulence – in the daytime mixed layer. However, observations indicate that the daytime mixed layer is characterized by strong thermals and associated turbulent eddies that span the depth of the ABL (e.g., Fig. 2). Thus, the inability of local closure parameterizations to *explicitly* resolve transport by large eddies limits their realism.

Eddy-Diffusivity Countergradient Approaches

The countergradient approach to parameterizing turbulent vertical mixing by large eddies has been used extensively since its inception in the 1980s. A conceptually straightforward countergradient parameterization is that which, until recently, was used within the NCEP Global Forecast System model. The Yonsei University (YSU) parameterization available in the WRF-ARW model is a variant of this parameterization.

In eddy-diffusivity countergradient approaches, the eddy covariance term for vertical mixing has the general form:

$$\overline{w'\xi'} = -K\left(\frac{\partial\bar{\xi}}{\partial z} - \gamma_\xi\right)$$

γ_ξ is a correction applied to the local gradient formulation to account for turbulent mixing by large eddies. In the GFS model, this correction applied only to the mass variables (heat and

moisture) in the ABL; otherwise, the correction term is set to zero. Where this correction term is zero, the formulation is identical to an eddy-diffusivity local closure. As a result, this non-local parameterization may be thought of as a 'corrected' local closure parameterization.

The empirical correction term takes the form given by Han et al. (2016):

$$\gamma_\xi = b\frac{\overline{\left(w'\xi'\right)_{sfc}}}{w_s h}$$

where w_s is the mixed-layer velocity scale, which is a function of the surface friction velocity u_{sfc}* and the wind profile evaluated at the top of the surface layer; b is an empirically defined constant; h is the ABL height; and $\overline{\left(w'\xi'\right)_{sfc}}$ is the surface sensible (for potential temperature) or latent (for water-vapor mixing ratio) heat flux, which is obtained from the surface layer parameterization. As the correction term is a function of a *surface* heat flux, this countergradient approach is one in which large eddies are assumed to be rooted in the surface layer, analogous to Fig. 8c.

The K used by this scheme is a function of the height above the ground z, the mixed layer velocity scale w_s, and the height of the ABL h (Han et al. 2016):

$$K = \frac{1}{\mathrm{Pr}}\kappa w_s z\left(1-\frac{z}{h}\right)^p$$

where Pr is the Prandtl number, $\kappa = 0.4$ is the von Karman constant, and $p = 2$ is an empirically defined constant. All other variables are as defined previously.

Eddy-Diffusivity Mass-Flux Approaches

Eddy-diffusivity mass-flux methods use a mass-flux parameterization to represent the non-local updraft transport of potential temperature and water-vapor mixing ratio in sub-grid-scale entraining and detraining thermals that are driven by surface sensible heating. An illustrative schematic of a turbulent ABL containing such a thermal is given by Fig. 9. This approach has its roots in cumulus parameterization, which first utilized mass-flux approaches in the 1980s, and was adapted to the more general challenge of turbulent vertical mixing beginning in the late 2000s. More complex mass-flux formulations consider non-local momentum and/or downdraft transport, the latter such as that associated with boundary-layer stratocumulus clouds. This approach represents the current state-of-the-art for boundary-layer parameterizations.

The flux covariance of vertical velocity w with any prognostic variable ξ can be written as:

$$\overline{w'\xi'} = a_u\left(\overline{w'\xi'}\right)_u + \left(1-a_u\right)\left(\overline{w'\xi'}\right)_e + a_u\left(1-a_u\right)\left(w_u - w_e\right)\left(\xi_u - \xi_e\right)$$

where subscripts of *u* and *e* denote updraft and environment (e.g., the part of a grid cell outside of a thermal), respectively, and a_u is the fractional area of a grid cell within a thermal. The right-side terms represent turbulence *in* the thermal, turbulence *outside* the thermal, and organized turbulence between the thermal and its surroundings.

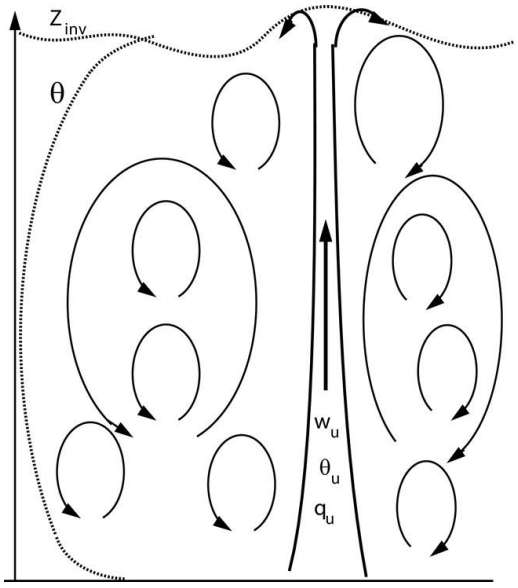

Figure 9. Sketch of a thermal (i.e., dry convective updraft) embedded in a turbulent ABL. Figure reproduced from Siebesma et al. (2007), their Fig. 1.

With $\overline{w} = a_u w_u + \left(1-a_u\right) w_e$ (representing the weighted average between the updraft velocity, which is inherently on the sub-grid-scale, and the environment's vertical velocity), solving for w_e and substituting into the above equation, we obtain:

$$\overline{w'\xi'} = a_u\left(\overline{w'\xi'}\right)_u + \left(1-a_u\right)\left(\overline{w'\xi'}\right)_e + a_u\left(w_u - \overline{w}\right)\left(\xi_u - \xi_e\right)$$

Given the typically small area (relative to that of a grid cell) covered by a thermal, $a_u << 1$, which we can use to neglect the first right-side term and rewrite the second right-side term. If we further assume that $\xi_e \approx \overline{\xi}$, we obtain:

$$\overline{w'\xi'} \approx \left(1-a_u\right)\left(\overline{w'\xi'}\right)_e + M\left(\xi_u - \overline{\xi}\right)$$

where $M \equiv a_u\left(w_u - \overline{w}\right) \approx a_u w_u$ (as $\overline{w} \approx 0$) and is defined as the mass flux, the product of the updraft area (related to mass) and the updraft velocity. Eddy-diffusivity mass-flux approaches

use an eddy-diffusivity approach for the first right-side term, assumed to be associated with local mixing in stable to weakly unstable ABLs, and a mass-flux approach for the second right-side term, assumed to be associated with non-local mixing in unstable ABLs. The eddy-diffusivity portion of the parameterization typically follows one of the approaches for specifying *K* described earlier in the notes.

The mass-flux portion of the parameterization begins by initializing a thermal with a potential temperature that is locally slightly warmer than its surroundings, e.g.,

$$\theta_{u,z_1} = \overline{\theta_{z_1}} + \alpha \frac{\overline{w'\theta_s'}}{\sigma_{w,z_1}}$$

where z_1 is the height of the lowest above-ground model level, $\overline{w'\theta_s'}$ is the surface sensible heat flux (obtained from a surface-layer parameterization), σ_{w,z_1} is the empirically estimated standard deviation of the turbulent vertical velocity at the lowest model level, and α is an empirical coefficient set to 1.

As a thermal grows upward, it is assumed to obey the following equations for M and ξ:

$$\frac{1}{M}\frac{\partial M}{\partial z} = \varepsilon - \delta$$

$$\frac{\partial M \xi_u}{\partial z} = \varepsilon M \overline{\xi} - \delta M \xi_u + a_u F_{\xi_u}$$

where ε is the entrainment rate (i.e., from the surroundings), δ is the detrainment rate (i.e., to the surroundings), and F_{χ_u} represents external source and sink terms acting on ξ_u in the updraft (e.g., radiation, advection, pressure forces, etc.). The first equation describes how the mass flux changes with height – increasing if entrainment exceeds detrainment – whereas the second describes how the mass flux of ξ changes with height – itself related to the balance between entrainment from the environment, detrainment from the updraft, and external source and sink terms.

For $\xi_u = \theta_u$ or $\xi_u = q_{v,u}$, external sources are typically neglected by assuming that their associated changes are zero on turbulent scales. In such cases, the equations above can be combined to obtain:

$$\frac{\partial \xi_u}{\partial z} = -\varepsilon\left(\xi_u - \overline{\xi}\right)$$

This shows that ξ_u returns toward $\overline{\xi}$ with height at a rate proportional to the entrainment rate. For θ_u, one can solve this equation upward from $z = z_1$, given that we know the grid-scale-resolved $\overline{\theta}$ from the model and θ_{u,z_1} from the equation given above, if we have an appropriate parameterization for ε. The same is true for $q_{v,u}$ if an initial q_{v,u,z_1} is specified (e.g., from the surface latent heat flux) since we know the grid-scale-resolved $\overline{q_v}$ from the model.

For the momentum fields, of which we are chiefly concerned with the updraft velocity w_u since it controls the value of M (and boundary-layer height, at least in some implementations, which can be viewed as the height at which w_u becomes zero), the external source terms cannot be neglected. For w_u, the most important external forces are pressure, which conveniently scales with w_u^2, and buoyancy. Incorporating these forces into the budget equations and performing some algebraic manipulations, we obtain an equation for w_u:

$$\frac{\partial w_u^2}{\partial z} = -b_1 \varepsilon w_u^2 + b_2 B$$

where b_1 and b_2 are empirically determined coefficients and B is buoyancy:

$$B = g \frac{\left(\theta_{v,u} - \overline{\theta_v}\right)}{\overline{\theta_v}}$$

With an appropriate lowest-model-level initial condition for w_u (e.g., zero), the vertical variation in w_u – a function of buoyancy, pressure forces, and entrainment – can be computed.

This leaves two unknown parameters: entrainment rate ε and updraft area fraction a_u. The entrainment rate ε is typically parameterized using empirical relationships derived from LES data; in general, it is parameterized with highest rates near the surface and ABL top. The updraft area fraction a_u is often treated as a specified constant (~0.01-0.05 in kilometer-scale models, ~0.1-0.15 in coarser models), though scale-aware formulations that reduce a_u at finer scales (under the assumption that the model can explicitly resolve a greater percentage of thermal-driven turbulence as the horizontal grid spacing decreases) have recently been developed.

Interactions Between ABL and Other Parameterizations

An ABL parameterization must interact with several other physical parameterizations. Surface roughness is conveyed through land-use data provided to a land-surface parameterization. Latent and sensible heat fluxes are modulated both by properties of the underlying surface (as reflected by soil type, soil temperature, and soil moisture) and by shortwave radiation (as manifest through

both the diurnal cycle and cloud effects). Accurately representing the interface between the mixed layer and the surface layer beneath it requires that ABL parameterizations effectively interact with surface-layer parameterizations.

Furthermore, although the two do not interact with each other, it is helpful to keep in mind that explicit diffusion is used to represent all *horizontal* mixing above the ABL, whereas an ABL parameterization is used to represent all *horizontal and vertical* mixing in the ABL and only vertical mixing above the ABL.

Practical Examples of Forecast Sensitivity to ABL Parameterization

There are numerous published works in which forecast sensitivity to the choice of ABL parameterization has been evaluated. Here, we focus on a small subset of these works.

(1) Historical characteristics of local and non-local closures

Historical evaluations of local and non-local closure parameterizations suggest that vertical mixing is typically underrepresented by local closures and overrepresented by non-local closures. For local closures, this results in shallower ABLs that are too cool and moist, and thus too energetic (e.g., surface-based CAPE and CIN), relative to observations. For non-local closures, this results in deeper ABLs that are too warm and dry, and thus less energetic, relative to observations.

Illustrative examples are given by Bright and Mullen (2002, *Wea. Forecasting*) for daytime warm-season ABLs over Arizona (Fig. 10) and Stensrud and Weiss (2002, *Wea. Forecasting*) for a case study of the daytime ABL (Fig. 11). Note that not all errors depicted in the simulated profiles are exclusively associated with the ABL parameterization; errors in the model's initial conditions and other parameterizations can also contribute. Many subsequent investigators have obtained similar results to those depicted in Figs. 10-11.

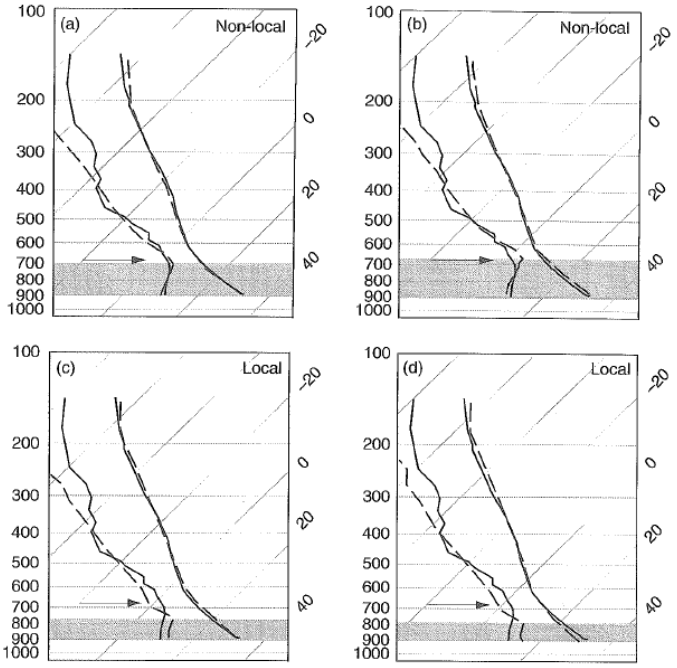

Figure 10. Simulated 12-h-forecast composite soundings (dashed lines) valid at 0000 UTC at Tucson, AZ from (a,b) non-local and (c,d) local closure parameterizations. The verifying observed soundings are depicted by the solid black lines. Gray shading indicates simulated ABL depth, while the arrow denotes observed ABL depth. Figure reproduced from Stensrud (2007), their Fig. 5.22, which was adapted from Fig. 11 of Bright and Mullen (2002).

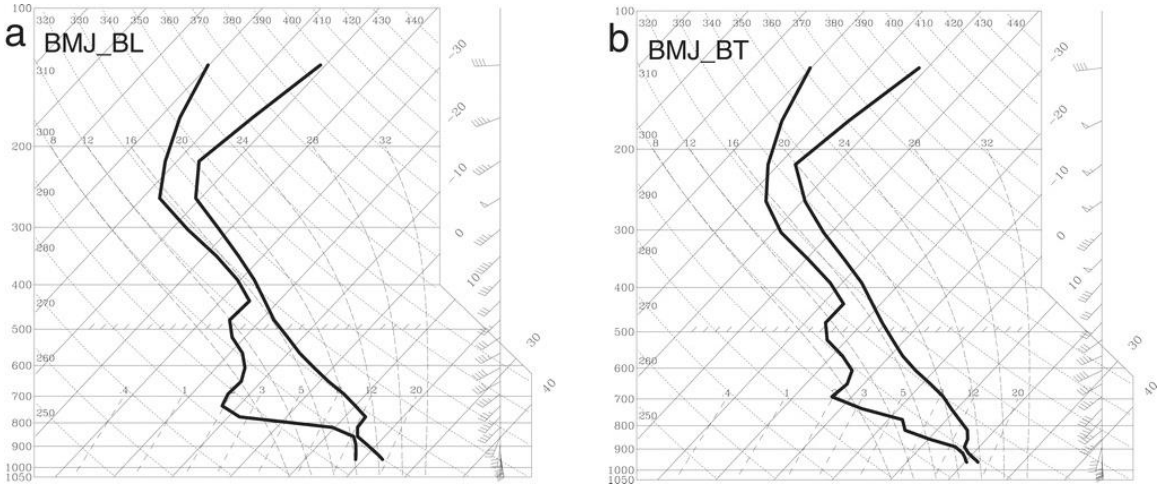

Figure 11. Simulated 24-h forecast soundings valid at 0000 UTC 4 May 1999 at Oklahoma City, OK from simulations utilizing a (a) non-local and (b) local closure parameterization. Figure reproduced from Stensrud and Weiss (2002), their Fig. 8. The verifying sounding is available from the University of Wyoming Atmospheric Sounding archive.

(2) Convection initiation: Schumacher (2015, *Mon. Wea. Rev.*)

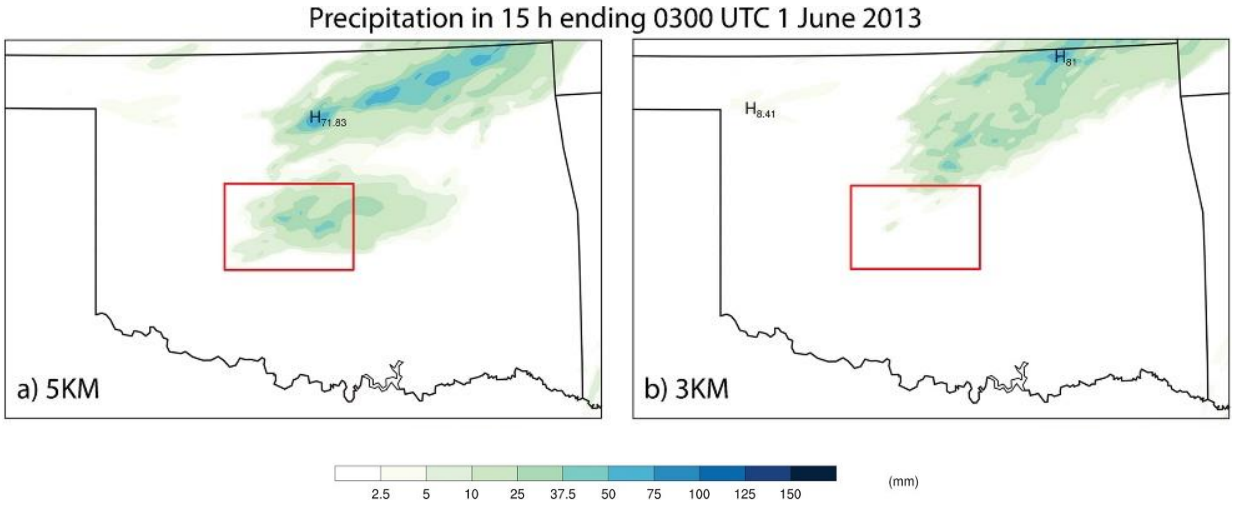

Figure 12. Accumulated precipitation (shaded in mm per the color bar) over the period 1200 UTC 31 May – 0300 UTC 1 June 2013 from otherwise identical simulations at Δx = 5 km (left) and Δx = 3 km (right). The red rectangle represents the area in which the El Reno supercell initiated and evolved late in this 15-h period. Figure reproduced from Schumacher (2015), their Fig. 11.

This study examines the grid-spacing–dependence of convection initiation for the 31 May 2013 El Reno, OK tornadic supercell. Coarser yet still convection-allowing grid spacings of 4-5 km reliably simulated supercell initiation, whereas finer grid spacings of ≤ 3 km did not (Fig. 12). This is attributed to overly strong boundary-layer overturning circulations – in this case, associated with northeastward-propagating gravity waves – along and ahead of the dryline in simulations that use finer grid spacings (which parameterize and crudely resolve a portion of the associated turbulence). Through mixing with the drier free atmosphere above, these circulations reduce ABL water-vapor mixing ratio ahead of the dryline (Fig. 13), resulting in a thermodynamic environment unable to support supercell initiation for the given external forcing. Sensitivity simulations and Ching et al. (2014, *Mon. Wea. Rev.*) indicate that these issues are most problematic for local closures (e.g., the Mellor-Yamada-Janjic scheme used in this study) as compared to non-local closures (wherein the stability is not limited to that between adjacent vertical levels).

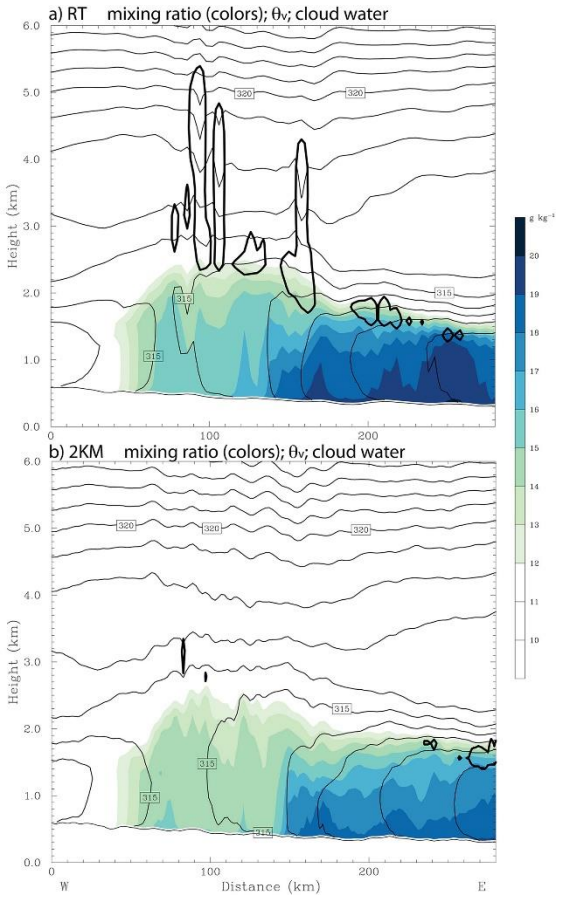

Figure 13. West-east vertical cross-sections (roughly across the red area in Fig. 12) of water-vapor mixing ratio (shaded in g kg^{-1} per the color bar), virtual potential temperature (thin contours in K), and cloud-water mixing ratio (thick contour at 0.05 g kg^{-1}; used to indicate precipitating features) at 2200 UTC 31 May 2013 from the (a) 4-km real-time and (b) 2-km simulations of the El Reno tornadic supercell. Figure reproduced from Schumacher (2015), their Fig. 18a-b.

(3) Dryline position: Clark et al. (2015, *Wea. Forecasting*)

Focusing on warm-season environments known to support severe convection, Clark et al. (2015) examine sensitivity in dryline position to ABL parameterization. In the composite mean, all ABL parameterizations are associated with an eastward bias in dryline position relative to observations. Given the general insight from the studies cited in (1), it is perhaps not surprising that the magnitude of this bias is largest with non-local closures and smallest with local closures (Fig. 14) since the dryline's position is a function of vertical mixing in the daytime ABL. An exception arises with the then-local-closure Mellor-Yamada-Nakanishi-Niino parameterization (which has since seen significant upgrades), wherein strong vertical mixing contributed to a large

eastward bias in the composite mean simulated dryline position. Errors in simulated composite vertical profiles of temperature, mixing ratio, and boundary layer depth generally follow from those described in (1) above.

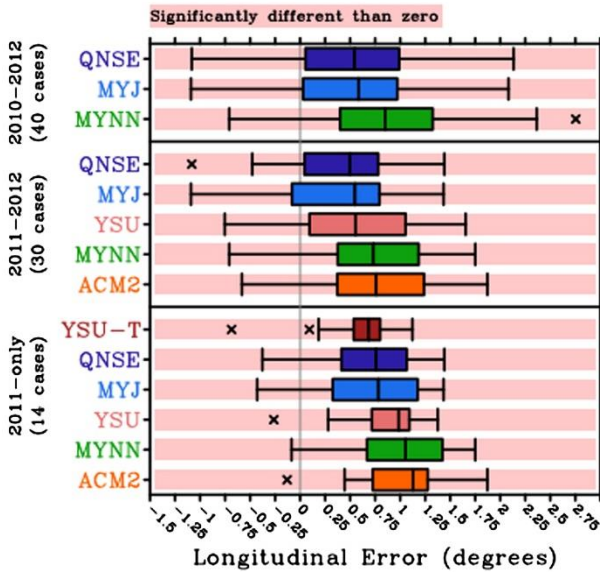

Figure 14. Box-and-whiskers plots of longitudinal error in simulated dryline position relative to observations (positive values denote an eastward bias) for simulations of warm-season environments supportive of thunderstorms. The median error is denoted by the solid vertical line through each box, which itself depicts the interquartile range. Outliers are defined as cases where the longitudinal error magnitude exceeds 1.5 times the interquartile range. The YSU and ACM2 schemes are non-local closures, whereas the MYJ, MYNN (at the time of this study), and QNSE schemes are local closures. Figure reproduced from Clark et al. (2015), their Fig. 6.

(4) Idealized tropical cyclone simulations: Hill and Lackmann (2009, *Mon. Wea. Rev.*)

This study examines the sensitivity in the maximum intensity of an idealized tropical cyclone to paired atmospheric boundary layer and surface-layer parameterizations. The moisture exchange coefficient between the ocean and the atmosphere is larger with the surface layer model tied to the Mellor-Yamada-Janjic (MYJ) local parameterization than with the surface layer model tied to the YSU non-local parameterization (Fig. 15). This results in larger surface latent heat fluxes in the MYJ-based simulations, in turn leading to stronger tropical cyclones in the MYJ simulations relative to the YSU simulations (since surface latent heat fluxes are the primary energy source for tropical cyclones).

Note that ABL parameterizations are typically designed, or tuned, to work with a specific surface layer model. How the surface layer model represents heat, moisture, and momentum exchange between the surface layer and the underlying surface exerts a significant control upon potential temperature, mixing ratio, and momentum in the surface layer. This influences turbulent vertical

mixing in both non-local and local closures. Thus, ABL parameterization performance must be evaluated in light of both it and its accompanying surface-layer parameterization.

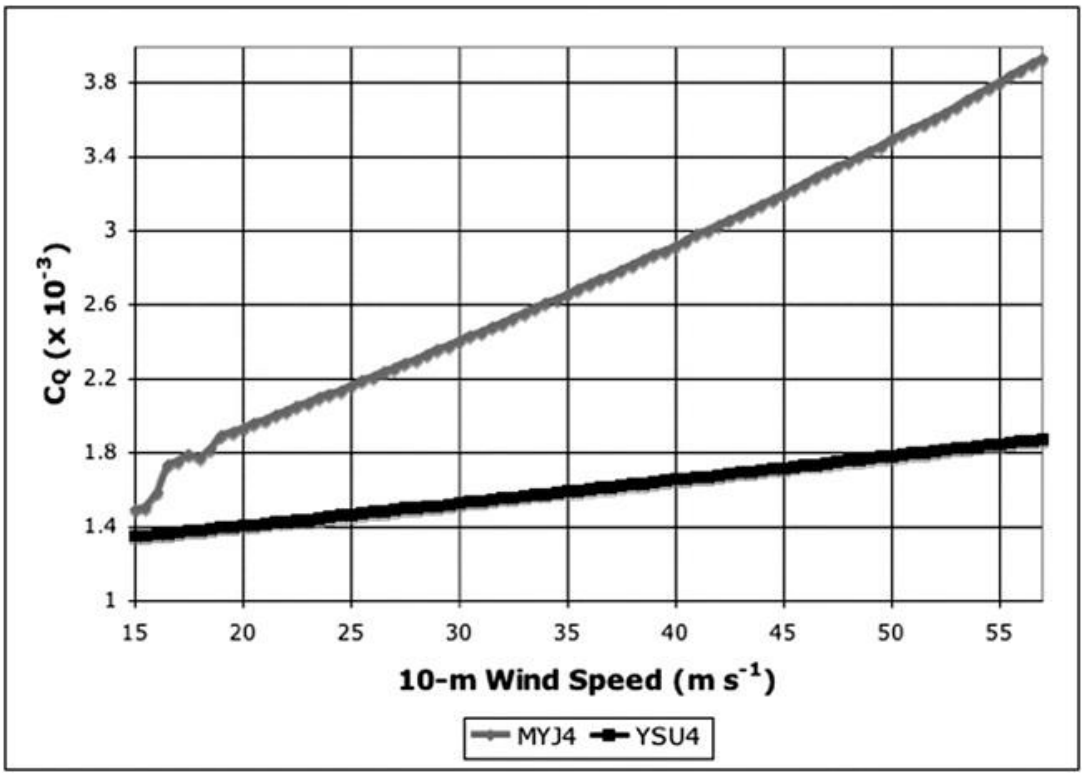

Figure 15. Moisture exchange coefficient (x10^{-3}; non-dimensional) as a function of 10-m wind speed (m s^{-1}) for the MYJ- (grey) and YSU-based (black) simulations. Figure reproduced from Hill and Lackmann (2009), their Fig. 6.